Dist: A

AD-A284 107

DOCUMENTATION PAGE

Form Approved
OMB No. 0704-0188

1)	2. REPORT DATE	3. REPORT TYPE AND DATES COVERED
	June 20, 1994	Final Report, 15 SEP91-29APR94

4. TITLE AND SUBTITLE
Reconstruction of Shapes from Shading and Shape Based Image Reconstruction Using Modern Nonlinear Analysis (U)

5. FUNDING NUMBERS
F 49620-91-C-0083
61102F
7981/DARPA

(1)

6. AUTHOR(S)
Stanley Osher

7. PERFORMING ORGANIZATION NAME(S) AND ADDRESS(ES)
Cognitech, Inc.
2800 - 28th St., Suite 101
Santa Monica, CA 90405

DTIC
ELECTED
SEP 08 1994
F

8. PERFORMING ORGANIZATION REPORT NUMBER
Report #31
AFOSR-TR- 94 0518

9. SPONSORING/MONITORING AGENCY NAME(S) AND ADDRESS(ES)
USAF, AFSC
AFOSR
110 Duncan, Suite B115
Bolling AFB, DC 20332-0001

10. SPONSORING/MONITORING AGENCY REPORT NUMBER

11. SUPPLEMENTARY NOTES

12a. DISTRIBUTION/AVAILABILITY STATEMENT
APPROVED FOR PUBLIC RELEASE:
DISTRIBUTION UNLIMITED
A

12b. DISTRIBUTION CODE
UL

13. ABSTRACT (Maximum 200 words)

Shape based restoration, frame fusion, stereo matching, reconstruction of shapes-from-shading, photometric stereo and video processing were successfully integrated into a partial differential equations based framework. Tools from the theory viscosity solutions, nonoscillatory approximations, and calculus of variations were used to develop state-of-the-art algorithms in these areas.

1997 94-29022

94 9 0C 092

DTIC QUALITY INSPECTED 3

14. SUBJECT TERMS	15. NUMBER OF PAGES
Frame fusion, stereo matching, photometric stereo, shape-from-shading, ENO, denoising, restoration	18
	16. PRICE CODE

17. SECURITY CLASSIFICATION OF REPORT	18. SECURITY CLASSIFICATION OF THIS PAGE	19. SECURITY CLASSIFICATION OF ABSTRACT	20. LIMITATION OF ABSTRACT
unclassified	unclassified	unclassified	UL SAR

Cognitech researchers and consultants successfully worked on quite a number of topics culminating in an accurate reconstruction of shapes from shading and shape based image restoration, as well as frame fusion, stereo matching, and video processing. These were integrated into a forensic image and video processing system which achieved great success in the legal fields [1,2].

Personnel who worked on this effort, listed in alphabetical order, were P.-L. Lions, M. Lyublinsky, J.-M Morel, S. Osher, L. Rudin, and P. Yu.

We began with the classical problem of a surface illuminated by a single distant source. The surface is given by the equation

$$z = u(x, y). \tag{1}$$

The normal $N = \frac{(-u_x, -u_y, 1)}{\sqrt{1+u_x^2+u_y^2}}$ and the intensity satisfies

$$I(x, y) = R(N). \tag{2}$$

In the simple, Lambertian case the equation becomes

$$\begin{aligned} I = \cos\theta &= (\alpha, \beta, -\gamma) \cdot (-N) \\ &= \frac{\alpha u_x + \beta u_y + \gamma}{\sqrt{u_x^2 + u_y^2 + 1}}. \end{aligned} \tag{3}$$

This was first studied carefully in [11] under the direction of our consultant, Dr. Pierre-Louis Lions. Equation (3) can be solved numerically using the theory of viscosity solutions for Hamilton-Jacobi equations [5]. The numerical schemes used in [6] were only first order accurate, monotone methods. High order accurate essentially nonoscillatory (ENO) were devised in [9,10] by the principal investigator of this contract. The main idea comes from a uniqueness theorem in [11] concerning the viscosity solution of the Hamilton-Jacobi equation

$$H(x, y, \nabla u) = I\sqrt{1 + u_x^2 + u_y^2} - \alpha u_x - \beta u_y - \gamma = 0, \text{ in } \Omega \tag{4}$$

with $(-\alpha, -\beta, \gamma)$, the direction cosines of the distant light source.

Given a level surface, $u = 0$ on $\partial\Omega$, we wish to solve (4). There is a lack of uniqueness as exemplified in one space dimension for overhead light ($\gamma = 1$). If $\Omega = \{x, 0 \le x \le 1\}$, given $u = 0$ at $x = 0$ or $x = 1$, we take $I = \frac{1}{\sqrt{1+(1-2x)^2}}$. Then two possible solutions are $u = \pm(x(1-x))$. This is visually an obvious fact to any observer. The uniqueness comes from the knowledge of the shape $u(x_0, y_0)$ where $I(x_0, y_0) = 1$.

Here $u_x = \pm\sqrt{\frac{1}{I^2} - 1}$ vanishes when $I = 0$. We generally need to impose the value of u at such points, subject of course to a compatibility condition. In this case we need

$$\begin{aligned} -\frac{1}{4} = -\max\left(\int_0^{\frac{1}{2}} \sqrt{\frac{1}{I^2} - 1}dx, \int_{\frac{1}{2}}^1 \sqrt{\frac{1}{I^2} - 1}dx\right) &\le u\left(\frac{1}{2}\right) \\ \le \max\left(\int_0^{\frac{1}{2}} \sqrt{\frac{1}{I^2} - 1}dx, \int_{\frac{1}{2}}^1 \sqrt{\frac{1}{I^2} - 1}dx\right) &= \frac{1}{4}. \end{aligned} \tag{5}$$

This condition generalizes easily.

We have derived higher order ENO codes which dramatically increase the accuracy obtained in [1]. Also, based on [8,12] we have devised a marching algorithm using the distance function which gives very rapid convergence to the solution of (4) with the appropriate conditions at points of maximum intensity.

Next, we used the results described by our consultant in [7] to handle shadows and more general boundary conditions for this Lambertian case. They are best described by appealing to the unsteady evolution problem

$$u_t = I\sqrt{1+u_x^2+u_y^2} - \alpha u_x - \beta u_y - \gamma. \tag{6}$$

If the left boundary is $x = 0$, then classical theory of initial-boundary value problems for hyperbolic equations indicate that a boundary condition should be imposed if

$$\frac{u_x I}{\sqrt{1+u_x^2+u_y^2}} < \alpha$$

or, at steady state, if

$$\beta u_x u_y + \gamma u_x - \alpha - \alpha u_y^2 < 0. \tag{7}$$

Different types of boundary conditions arise in the presence of shadows and grazing rays. They can be exemplified by the one dimensional case in which the exact surface is

$$\begin{aligned} u &\equiv -\sqrt{1-a^2} + \sqrt{1-x^2} \quad \text{for } |x| \le a \\ u &\equiv 0 \qquad\qquad\qquad\quad \text{if } |x| > a. \end{aligned} \tag{8}$$

We wish to solve

$$u_t = I\sqrt{1+u_x^2} - \alpha u_x - \gamma \tag{9}$$

to steady state.

The first case is that of an apparent contour. This happens when we have overhead light with $\gamma = 1$, $\alpha = 1$, and

$$\begin{aligned} I &= \sqrt{1-x^2} \quad \text{if } |x| \le 1 \\ I &\equiv 1 \qquad |x| > 1. \end{aligned}$$

Thus we solve

$$u_t = \sqrt{1-x^2}\sqrt{1+u_x^2} - 1, \quad |x| \le 1.$$

This has a characteristic boundary at $x = \pm 1$. Thus we impose no boundary conditions there. We do impose $u = 1$ at $x = 0$ because $I(0) = 1$.

More generally at $x = -a$, we need no boundary condition if $\frac{a}{\sqrt{1-a^2}} = u_x > \frac{\alpha}{\gamma} = \frac{\alpha}{\sqrt{1-\alpha^2}} \Leftrightarrow a > \alpha$. At $x = -\alpha$, $u_x = \frac{\alpha}{\gamma} \Leftrightarrow I = 1$. Thus we need to prescribe $u(-\alpha) = \sqrt{1-\alpha^2} - \sqrt{1-a^2}$ at a grazing light edge, e.g. $x = \gamma$, $u_x(\gamma) = -\frac{\gamma}{\alpha}$.

Finally at a shadow edge, i.e. at $x = \frac{1}{\alpha}$, we need to prescribe $u(\frac{1}{\gamma}) = u(\gamma) - \alpha$.

We have also developed methods for more complicated models involving highlights. Here

$$I(x,y) = \cos\theta + c(\cos\theta)^m \tag{10}$$

for c, m functions of the metal. Thus the Hamilton-Jacobi equation to be solved is

$$I(x,y) = \frac{\alpha u_x + \beta u_y + \gamma}{\sqrt{1+u_x^2+u_y^2}} + c\left[\frac{\alpha u_x + \beta u_y + \gamma}{\sqrt{1+u_x^2+u_y^2}}\right]^m.$$

The numerical methods used to solve the Hamilton-Jacobi equations were high order ENO as developed in [9,10]. The equation is always of the form

$$u_t = -H(x, y, u_x, u_y). \tag{11}$$

Monotone schemes are of the form

$$u_{ij}^{n+1} = u_{ij}^n - \Delta t \hat{H}(x_i, y_j, D_+^x u_{ij}^n, D_-^x u_{ij}^n; D_+^y u_{ij}^n, D_-^y u_{ij}^n) \tag{12}$$

with $\hat{H}(u, u, U, U) = H(u, U)$ and $\hat{H}(\uparrow, \downarrow; \uparrow, \downarrow)$ denotes its monotonicity.

Another speed up of the steady state calculation comes via nonlinear SOR. This works because of monotonicity. Godunov's scheme is such that we can analytically solve for the value of u, j at the central point. For high order ENO methods we rewrite the steady state algorithm as

$$\hat{H}^{\text{monotone}} = \hat{H}^{\text{monotone}} - \hat{H}^{\text{ENO}}. \tag{13}$$

We lag the right side of this equation and update using nonlinear SOR on the left. This algorithm is quite fast.

Figures 1-16 demonstrate the success of this approach for a single-view shape-from-shading.

Our next effort concerned the problem of photometric stereo. There, the same Lambertian surface is viewed at different times of the day. Thus the goal is to find u, given measurements (which have some errors)

$$F^{(K)} = I^{(K)}\sqrt{1 + u_x^2 + u_y^2} - (\alpha^{(K)}u_x + \beta^{(K)}u_y + \gamma^{(K)}) = 0 \tag{14}$$

$$K = 1, \ldots, m.$$

The idea is to minimize the functional

$$\int_\Omega \Sigma \omega^{(K)} |F^{(K)}|^{2p} dx dy, \tag{15}$$

using weights $0 < \omega^{(K)}$. We also let $p \to \infty$ and use gradient descent and artificial time. Thus we seek steady solutions of

$$u_t = \sum_K \omega^{(K)} \Big\{ \text{Trace} \left[D^2 u \cdot \left[\frac{\partial F^{(K)}}{\partial p}(x, \nabla u) \otimes \frac{\partial F^K}{\partial p}(x, \nabla u \right] \right] + \frac{\partial F^{(K)}}{\partial p}(x, \nabla u) \cdot \frac{\partial F^{(K)}}{\partial x}(x, \nabla u) \Big\}$$

Unfortunately, there is no uniqueness in general. We could, for example, take $I^{(i)} = \frac{\gamma^{(i)}}{\sqrt{2}}$, $i = 1, 2$ with $\beta^{(1)} = \sqrt{1 - (\gamma^{(1)})^2}$, $\beta^{(2)} = -\sqrt{1 - (\gamma^{(2)})^2}$, then $u \equiv \pm x$ are both solutions. Also any continuous piecewise linear function of slope 1+1, is a Lipschitz continuous solution. In fact, for any planar solution of the form

$$u = c_1 x + c_2 y + c_3.$$

Then the function

$$v = d_1 x + d_2 y + d_3$$

is also a solution if

$$\alpha^{(1)}c_1 + \beta^{(1)}c_2 + I^{(1)}\sqrt{1 + c_1^2 + c_2^2} = \alpha^{(2)}d_1 + \beta^{(2)}d_2 + I^{(2)}\sqrt{1 + d_1^2 + d_2^2}.$$

From a geometric point of view, the statement is that two planes are both solutions iff all light sources lie on the great circle bisecting the angle between them. In general, $\exists$ at most two planar solutions and in particular, *only one if there are at least three light sources which are not in the same plane.*

This they is valid for the weights $\omega^{(K)} \equiv 1$; however we use $\omega^{(K)}[F^{(K)}]^{\frac{1}{2}}[I^{(K)}]^{\frac{1}{2}}$ in our experiments.

The steady state problem is a degenerate quasilinear elliptic equation. It degenerates in direction ξ (at $x, p = \nabla u(x)$) if $\frac{\partial F^{(K)}}{\partial p}(x, \nabla u) \cdot \xi = 0$ for all K. This is equivalent to

$$I^{(K)} \frac{p \cdot \xi}{\sqrt{1+|p|^2}} + \ell^{(K)} \xi = 0 \; (\ell^{(K)} = -(\alpha^{(K)}, \beta^{(K)}))$$

or

(E)
$$\frac{I^{(K)} p}{\sqrt{1+|p|^2}} + \ell^{(K)}$$

are all collinear.

An example of this is for one overhead light, $p(x_0) = 0$, $\ell^{(1)} = 0$. The second light is arbitrary.

Recall our counter example to uniqueness

$$\ell^{(1)} = \begin{pmatrix} 0 \\ \beta^{(1)} \end{pmatrix}, \ell^{(2)} = \begin{pmatrix} 0 \\ \beta^{(2)} \end{pmatrix}, \; \beta^{(1)} \neq \beta^{(2)}$$
$$I^{(1)} = \frac{\gamma^{(1)}}{\sqrt{2}}, \; u(x, y) = \pm x.$$

If we check condition (E) for $u \equiv x$ we have

$$\begin{pmatrix} \frac{I^{(1)}}{\sqrt{2}} \\ \beta^{(1)} \end{pmatrix} = \begin{pmatrix} \frac{\gamma^{(1)}}{2} \\ \beta^{(1)} \end{pmatrix} \| \begin{pmatrix} \frac{\gamma^{(2)}}{2} \\ \beta^{(2)} \end{pmatrix}$$

or

$$\beta^{(2)} \sqrt{1-(\beta^{(1)})^2} = \beta^{(1)} \sqrt{1-(\beta^{(2)})^2}.$$

Thus $\beta^{(1)}$ and $\beta^{(2)}$ have the same sign $\Rightarrow \beta^{(1)} = \beta^{(2)}$. This is a contradiction, thus we have uniform ellipticity here.

We have proven the following.

Theorem: *Given a maximum principle satisfying boundary condition, the evolution equation* (16) *is a well-posed initial value problem in the sense of viscosity solutions, even if there are degeneracies.*

Remark: Two lights are collinear when

$$\frac{Ip}{\sqrt{1+|p|^2}} + \ell = 0$$

for one and

$$p = \nabla u \text{ solves } I\sqrt{1+|p|^2} = \ell \cdot p + \gamma.$$

This is equivalent to $I = 1$, $p = -\frac{\ell}{\gamma}$, which is the precise loss of uniqueness in the single view case discussed earlier.

Additionally, if $p = \nabla u$ for a solution u then

$$(D^2u)\frac{\partial F^{(i)}}{\partial p} + \frac{\partial F^{(i)}}{\partial x} = 0.$$

If at $(x_0, \nabla u(x_0))$, $\frac{\partial F^{(i)}}{\partial x} = 0$, this implies $\Rightarrow D^2u(x_0)$ has one zero and one nonzero eigenvalue. Then (E) is valid at $(x^0, \nabla u(x_0))$ with a direction of degeneracy which corresponds to a nonzero eigenvalue.

In general, the operator can be degenerate since the initial condition is arbitrary. An example occurs if $p = \nabla u_0(x_0) = 0$. Then (E) occurs if the $\ell^{(i)}$ are collinear (so the directions of light all lie on a great circle).

Our equation (16) can be derived as follows. If we set

$$\begin{aligned} & F^{(i)}(x, \nabla u) = 0 \\ \Rightarrow & D^2u \cdot \frac{\partial F^{(i)}}{\partial p} + \frac{\partial F^{(i)}}{\partial x} = 0 \\ \Rightarrow & \text{Trace } \left(D^2u \left(\frac{\partial F^{(i)}}{\partial p} \otimes \frac{\partial F^{(i)}}{\partial p} \right) \right) \\ & + \frac{\partial F^{(i)}}{\partial p} \cdot \frac{\partial F^{(i)}}{\partial x} = 0. \end{aligned}$$

We obtain the right side of (16) by summing over (i).

Another derivation comes from considering the least L^p weighted norm of the error and letting $p \to \infty$. This leads us to natural boundary conditions.

Figures 17-24 show the results of our photometric stereo algorithm on real data.

An important problem relating to reconstruction of shapes involves stereo matching. We are given two views of the same images from different cameras. We call the intensity functions $L(x, y)$ and $R(x, y)$, and we seek to find matching functions $u(x, y)$, $v(x, y)$ so that $L(x + u(x, y), y + \nu(x, y))$ is as close as possible to $R(x, y)$.

Our approach is based on L^1 minimization

$$\min \int |L(x + u(x, y), y + \nu(x, y)| - R(x, y)| dx dy. \tag{17}$$

This is not sufficiently regularized - there are many possible solutions. We modify this by

$$\begin{aligned} \min \int & L(x + u(x, y), y + \nu(x, y)) - R(x, y)| dx dy \\ & + F(L, R, u, v, x, y). \end{aligned} \tag{18}$$

F is a complicated function related to the constraints.

Solving this problem directly via gradient descent will usually lead to a local minimum. We thus take a coarse to fine procedure to lead to our desried solution. We start by replacing $L(x, y)$ and $R(x, y)$ by blurred versions: $L_\sigma = G_\sigma * L$, $R_\sigma = G_\sigma * R$, where

$$G_\sigma = G_0 e^{-\frac{(x^2+y^2)}{\sigma^2}}$$

and $*$ denotes convolution.

We gradually reduce the variance σ and use the iteration result as an initial guess for a smaller σ. We thus can successfully approach the global minimum of this functional.

The algorithm is as follows:

Initial guess σ_0, u, v, for σ_0 large enough. Find new u, v by minimizing (18) with L and R replaced by L_σ, R_σ, reduce σ and iterate again.

The Euler-Lagrange equations for this functional show that when $\nabla L_\sigma \cdot \nabla R_\sigma < 0$, the solution procedure may lead to spurious minima. We remove this term when the sign turns negative.

The scaling is important in our minimization procedure. This leads to severe time step resolutions in our numerical method. We fix this by dynamically rescaling via an arc tangent function.

We note also that u and v can be discontinuous. The regularization term in F might prevent this from developing. These discontinuities in the matching functions are related to edges in the images. We used ENO schemes near discontinuities with good results.

Additionally, if L and R are flat, u and v can be assumed to be smooth. Thus the coefficients of the viscosity terms coming from F are large in flat regions and small near edges.

We also devised a morphological matching method concentrating on image features, i.e. the level set directions and curvature. We again let $L(x, y)$ and $R(x, y)$ be the intensity function of two images. Let $u(x, y)$ and $v(x, y)$ be the matching function between these two images. For the statement "match level set directions", we mean:

$$\min_{u,v} \int F_1(x, y, u, u_x, u_y, v_x, v_y, L, R) dx dy$$

where

$$F_1(x, y, u, u_x, u_y, v_x, v_y, L, R) = 1 - \frac{\nabla L(x+u, y+v)}{|\nabla L(x+u, y+v)|} \cdot \frac{\nabla R(x, y)}{|\nabla R(x, y)|}$$

or

$$F_1 = 1 - \frac{[L_x(1+u_x) + L_y v_x]R_x + [L_x u_y + L_y(1+v_y)]R_y}{\sqrt{[L_x(1+u_x) + L_y v_x]^2 + [L_x u_y + L_y(1+v_y)]^2}\sqrt{R_x^2 + R_y^2}}$$

where $L_x \equiv L_x(x+u, y+v)$ and $L_y \equiv L_y(x+u, y+v)$.

In the region where the value of gradient is small, the direction is very unstable numerically. So a better choice of the functional is obtained by multiplying the above functional by the norm of the gradient. This yields the following modified functional:

$$F_1(x, y, u, u_x, u_y, v_x, v_y, L, R) =$$
$$\sqrt{[L_x(1+u_x) + L_y v_x]^2 + [L_x u_y + L_y(1+v_y)]^2}\sqrt{R_x^2 + R_y^2} - [L_x(1+u_x) + L_y v_x]R_x - [L_x u_y + L_y(1+v_y)]R_y.$$

The minimal point is reached when the gradient of the two images has the same direction. However this does not mean we get the correct matching. Minimizing the functional is just a necessary condition for matching, not a sufficient condition. For two images to be matched, we introduce second term of the functional – matching image curvature. We describe it as follows:

Let

$$F_2(x, y, u, v, u_x, v_x, u_{xx}, u_{xy}, u_{yy}, v_{xx}, v_{xy}, v_{yy}) = |K(L(x+u, y+v)) - K(R(x, y))|$$

where K is the curvature operator. By expanding the right hand side term, we get,

$$
\begin{aligned}
F_2 = \| \{ & (L_x^2 L_{yy} - 2L_x L_y L_{xy} + L_y^2 L_{xx})[(1+u_x)(1+\nu_y) - \nu_x u_y]^2 \\
& + L_x^3[(1+u_x)^2 u_{yy} - 2(1+u_x)u_y u_{xy} + u_y^2 u_{xx}] \\
& + L_y^3[(1+\nu_y)^2 \nu_{xx} - 2(1+\nu_y)\nu_x \nu_{xy} + \nu_x^2 \nu_{yy}] \\
& + L_x^2 L_y[2(1+\nu_y)u_y u_{xx} - 2((1+u_x)(1+\nu_y) + \nu_x u_y)u_{xy} + 2(1+u_x)\nu_x u_{yy} \\
& \quad + u_y^2 \nu_{xx} - 2(1+u_x)u_y \nu_{xy} + (1+u_x)^2 \nu_{yy}] \\
& + L_x L_y^2[2(1+\nu_y)u_y \nu_{xx} - 2((1+u_x)(1+\nu_y) + \nu_x u_y)\nu_{xy} + 2(1+u_x)\nu_x \nu_{yy} \\
& \quad + \nu_x^2 u_{yy} - 2(1+\nu_y)\nu_x u_{xy} + (1+\nu_y)^2 u_{xx}]\}/ \\
& \{L_x^2[(1+u_x)^2 + u_y^2] + 2L_x L_y[(1+u_x)\nu_x + (1+\nu_y)u_y] + L_y^2[(1+\nu_y)^2 + \nu_x^2)]\}^{3/2} \\
& - (R_y^2 R_{xx} - 2R_x R_y R_{xy} + R_x^2 R_y^2)^{3/2} |
\end{aligned}
$$

Again, in the regions of smooth intensity we multiply the functional by the product of the norms of two gradients. Our modified functional becomes:

$$
\begin{aligned}
F_2(x, y, u, \nu, u_x, \nu_x, u_{xx}, u_{xy}, u_{yy}, \nu_{xx}, \nu_{xy}, \nu_{yy}) = & \\
& |(R_x^2 + R_y^2)^{3/2}\{(L_x^2 L_{yy} - 2L_x L_y L_{xy} + L_y^2 L_{xx})[(1+u_x)(1+\nu_y) - \nu_x u_y]^2 \\
& \quad + L_x^3[(1+u_x)^2 u_{yy} - 2(1+u_x)u_y u_{xy} + u_y^2 u_{xx}] \\
& + L_y^3[(1+\nu_y)^2 \nu_{xx} - 2(1+\nu_y)\nu_x \nu_{xy} + \nu_x^2 \nu_{yy}] \\
& \quad + L_x^2 L_y[2(1+\nu_y)u_y u_{xx} - 2((1+u_x)(1+\nu_y) + \nu_x u_y)u_{xy} + 2(1+u_x)\nu_x u_{yy} \\
& \quad\quad + u_y l^2 \nu_{xx} - 2(1+u_x)u_y \nu_{xy} + (1+u_x)^2 \nu_{yy}] \\
& \quad + L_x L_y^2[2(1+\nu_y)u_y \nu_{xx} - 2((1+u_x)(1+\nu_y) + \nu_x u_y)\nu_{xy} + 2(1+u_x)\nu_x \nu_{yy} \\
& \quad\quad + \nu_x^2 u_{yy} - 2(1+\nu_y)\nu_x u_{xy} + (1+\nu_y)^2 u_{xx}]\} \\
& - \{L_x^2[(1+u_x)^2 + u_y^2] + 2L_x L_y[(1+u_x)\nu_x + (1+\nu_y)u_y] + L_y^2[(1+\nu_y)^2 + \nu_x^2)]\}^{3/2} \\
& (R_y^2 R_{xx} - 2R_x R_y R_{xy} + R_x^2 R_{yy}) |
\end{aligned}
$$

This term should play a more important role in the region where the direction of the gradients are close. This means we will multiply the above term by a function of the first term $g(F_1)$. Here g is small when F_1 is large and g is large when F_1 is small.

In order to match in the smooth region we need the regularization terms. In order for the procedure to converge, and overcome the noise sensitivity of the derivatives of intensity functions, we still use our larger scale matching procedure. In order to allow sharp jumps to develop, we still need an essentially nonoscillatory method for derivatives to avoid crossing the discontinuities. All these facts mean that our previous work still applies.

We have extended these techniques to multiple frames when many views of an image are given. In fact a key application comes in frame fusion of videos. Neighboring frames are given and information is used to reconstruct the central frame in an accurate manner. The algorithm is quite similar to our stereo matching method described above.

Figures 25-31 show the results of our stereo matching algorithm.

Figures 32-33 show the results of our frame fusion algorithm. The upper left picture in Figure 32 is the true "airplane" which was subsampled down to a factor of 16 and placed in the middle of 10 consecutive frames. The upper right shows the replicated image. Figure 33, upper right shows the greatly enhanced result via frame fusion. Figure 34 demonstrates via excerpts from the Los Angeles Times, the use of frame fusion in the legal area.

We are currently integrating the work on video processing done by our collaborators in [3] together with our frame fusion ideas. We believe that our method gives an interesting slant on the computation of apparent velocity.

Finally we mention that a shape based denoising algorithm is now mature. This is based on the regularization properties of both the single view, Hamilton-Jacobi approach and the parabolic equation approach obtained in the photometric stereo case.

Bibliography

[1] "Image Processing Makes Its Mark in Court", SIAM News, Vol. 26, 81 (Dec., 1993).

[2] "Battlefield in Courtroom Tool-Video De-Blurring", Leading Edge, AFOSR Magazine, (March 1994), pp. 18-19.

[3] L. Alvarez, F. Guichard, P.-L. Lions, and J.-M. Morel, "Axioms and Fundamental Equations of Image Processing", Arch. for Rat. Mech. Anal., Vol. 123, (1993), pp. 199-257.

[4] A. Chambolle, "Stereo Vision and Shape from Shading", preprint, U. of Paris IX, CEREMADE, (1992).

[5] M. Crandall and P.-L. Lions, "Viscosity Solutions of Hamilton-Jacobi Equations", Trans. Amer. Math. Sco., Vol. 271, (1983), pp. 1-42.

[6] M. Crandall and P.-L. Lions, "Two Approximations of Solutions of Hamilton-Jacobi Equations", Math. Comput., Vol. 43, (1984), pp. 1-19.

[7] P.-L. Lions, E. Rouy, and A. Tourin, "Shape-from-Shading, Viscosity Solutions and Edges", Numer. Math., Vol. 64, (1993), pp. 323-354.

[8] S. Osher, "A Level Set Formulation for the Solution of the Dirichlet Problem for Hamilton-Jacobi Equations", SIAM J. on Analysis, Vol. 24, (1993), pp. 1145-1152.

[9] S. Osher and J. Sethian, "Fronts Propagating with Curvature Dependent Speed. Algorithms Based on Hamilton-Jacobi Formulations", J. Comput. Phys., Vol. 79, (1988), pp. 12-49.

[10] S. Osher and C.-W. Shu, "High Order, Essentially Nonoscillatory Schemes for Hamilton-Jacobi Equations", SINUM, Vol. 28, (1991), pp. 907-922.

[11] E. Rouy and A. Tourin, "A Viscosity Solutions Approach to Shape from Shading", SINUM, Vol. 29, (1992), pp. 867-884.

[12] M. Sussman, P. Smereka, and S. Osher, "A Level Set Approach for Computing Solutions to Incompressible Two-Phase Flow", J. Comp. Phys., (1994), to appear.

6. Results:

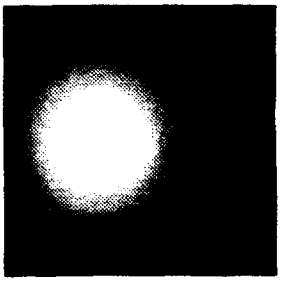

Fig. 1

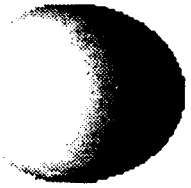

Fig. 2

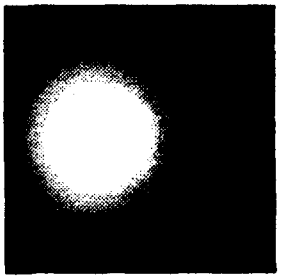

Fig. 3

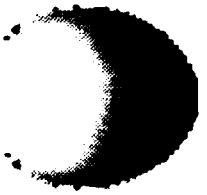

Fig. 4

Figure 1 is a semi-sphere shape, figure 2 is the shade of figure 1, figure 3 is the reconstructed shape, and figure 4 is the shade reconstructed from figure 3.

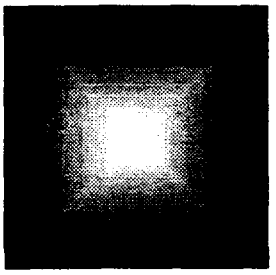

Fig. 5

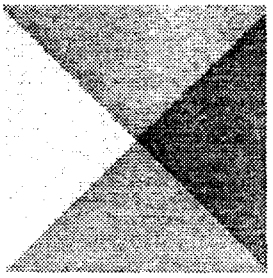

Fig. 6

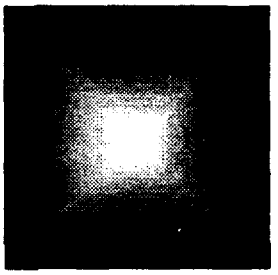

Fig. 7

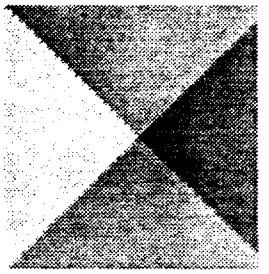

Fig. 8

Figure 5 is a shape of pyramid, its shade is shown on figure 6, the reconstructed shade and shape are shown on figure 7 and figure 8.

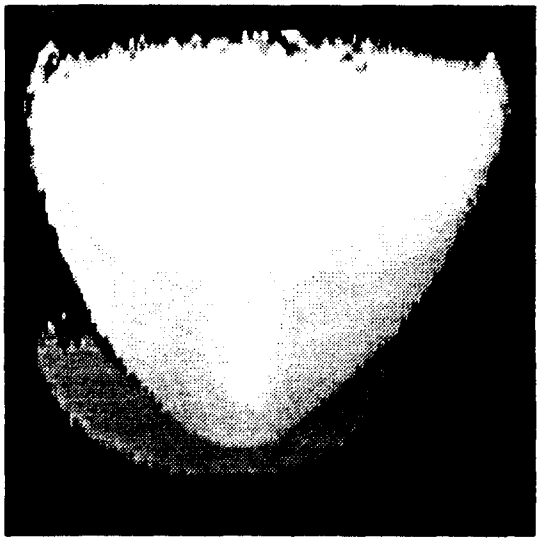

Fig. 9

Fig. 10

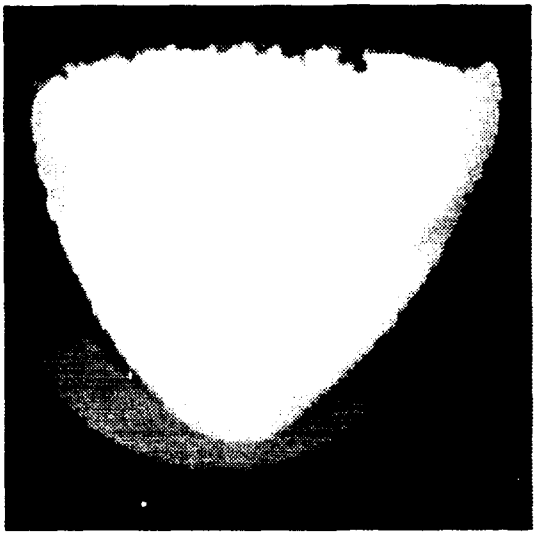

Fig. 11

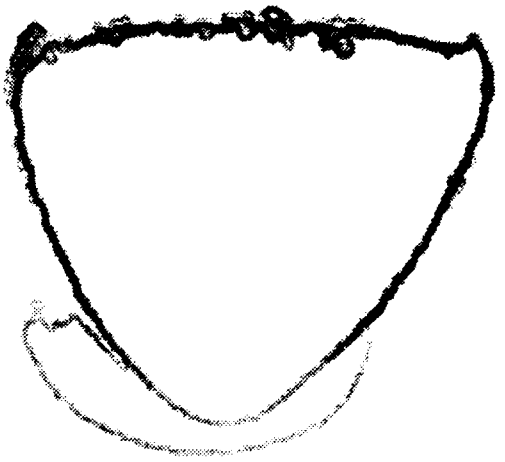

Fig. 12

Figure 9 is a shape of a face, figure 10 is the shade of the face with over head lighting. Figure 11 and 12 is the reconstructed shape and shade from figure 10.

7. The shape from shading problem does not necessary take the form in (1.). It can take other form. For example, the eye-ball model where the intensity can be written as:

$I(t) = t + t^5$ where $t(x,y) = \dfrac{\alpha \cdot u_x + \beta \cdot u_y + \gamma}{\sqrt{u_x^2 + u_y^2}}$

The following is a example of reconstructing $u(x,y)$ from given $I(x,y)$.

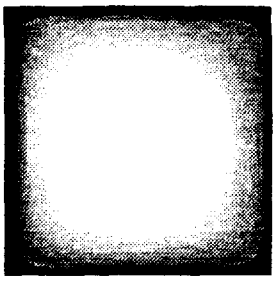

Fig. 13

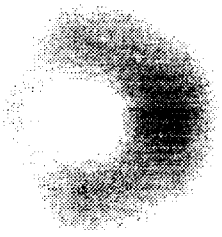

Fig. 14

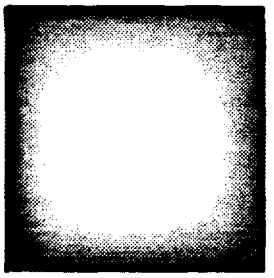

Fig. 15

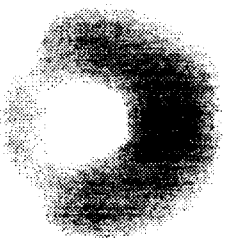

Fig. 16

Figure 13 is the original shape, figure 14 is the shade of figure 13 with eye-ball model. Figure 15 and 16 are the reconstructed shape and shade.

Photometric Stereo

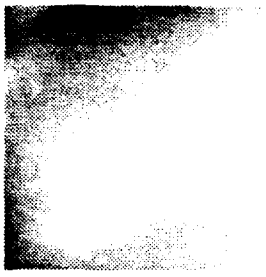

Fig. 17

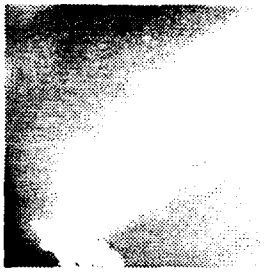

Fig. 22

Fig. 18

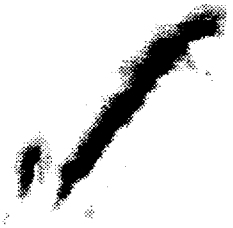

Fig. 19

Fig. 20

Fig. 21

Figure 17 is the shape of a mountain, Figure 18, 19, 20 and 21 are four shades corresponding to four different light directions. Figure 22 is the reconstructed shape of the mountain using figure 18 to 21.

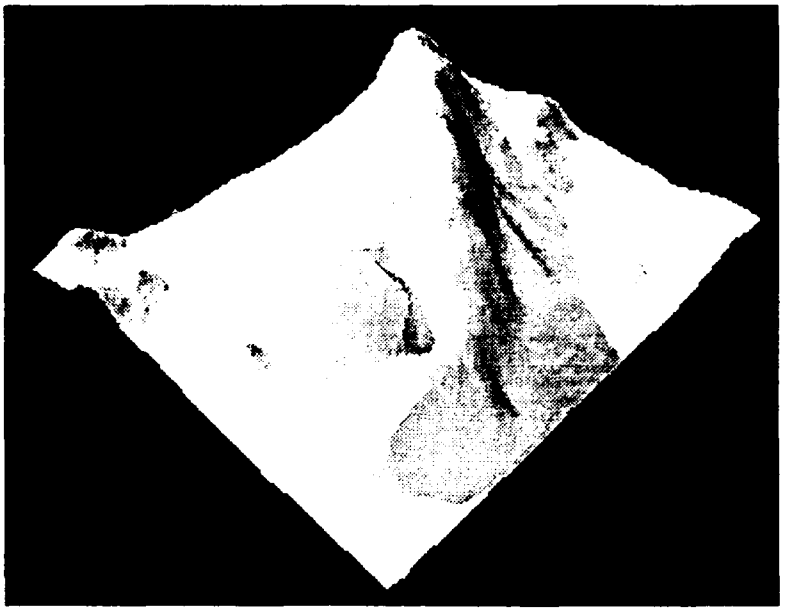

Fig. 23 Three dimensional view of the shape in figure 17

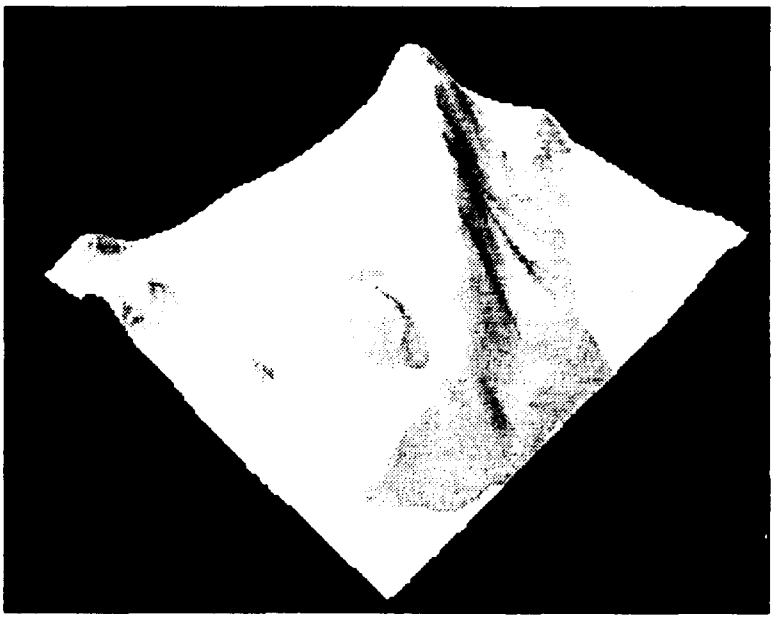

Fig. 24 Three dimensional view of the reconstructed shape in figure 22

Stereo Matching

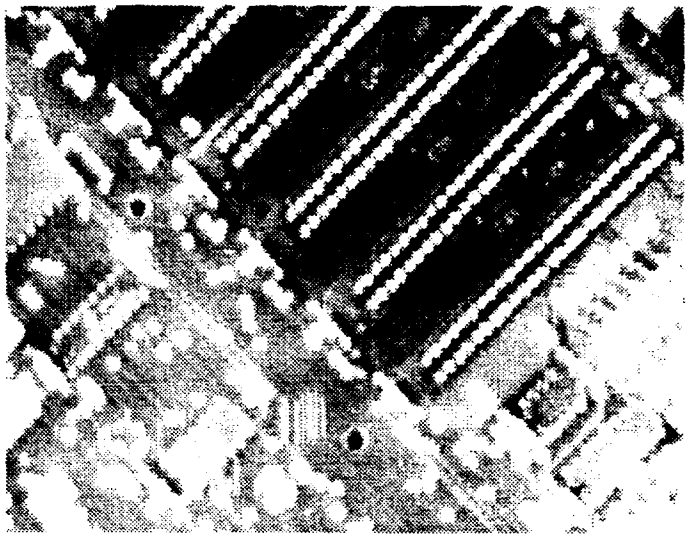

Fig. 25 Part of a circuits board (left view)

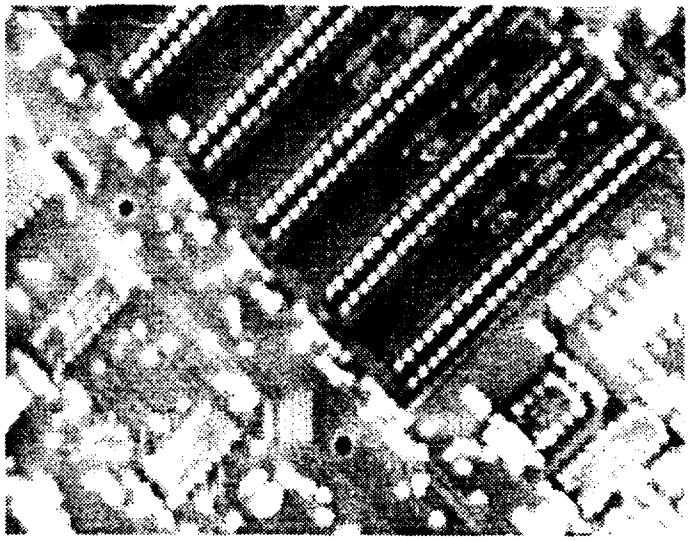

Fig. 26 Part of a circuits board (right view)

Fig. 27 Matching function [u(x,y)] of fig. 25 and 26.

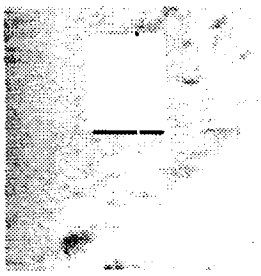

Fig. 28

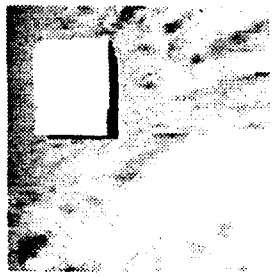

Fig. 29

Image pair of a mountain with building

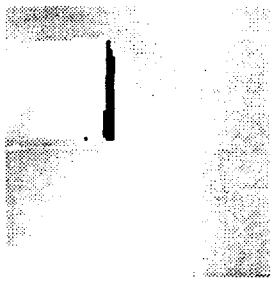

Fig. 30 Matching function u(x,y) of image pair 28 and 29

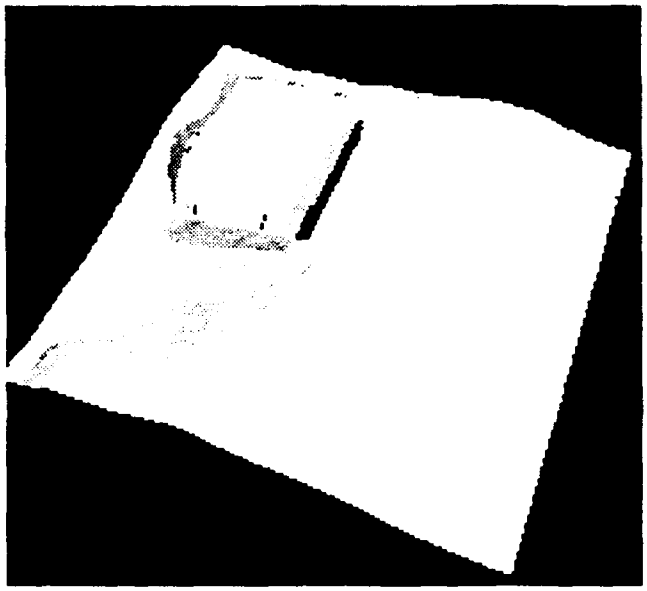

Fig. 31 Three dimensional view of u(x,y) in figure 30

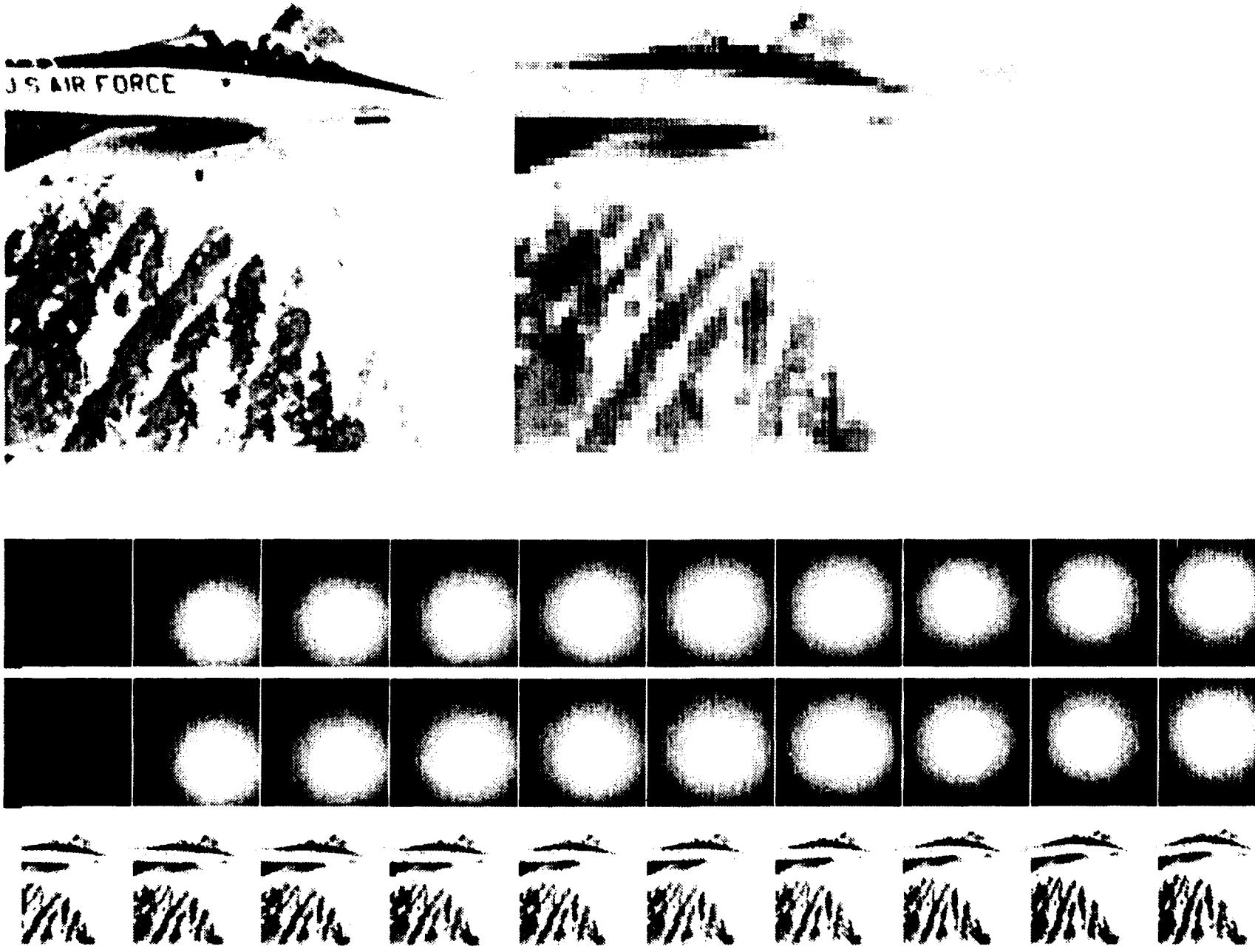

Figure 32

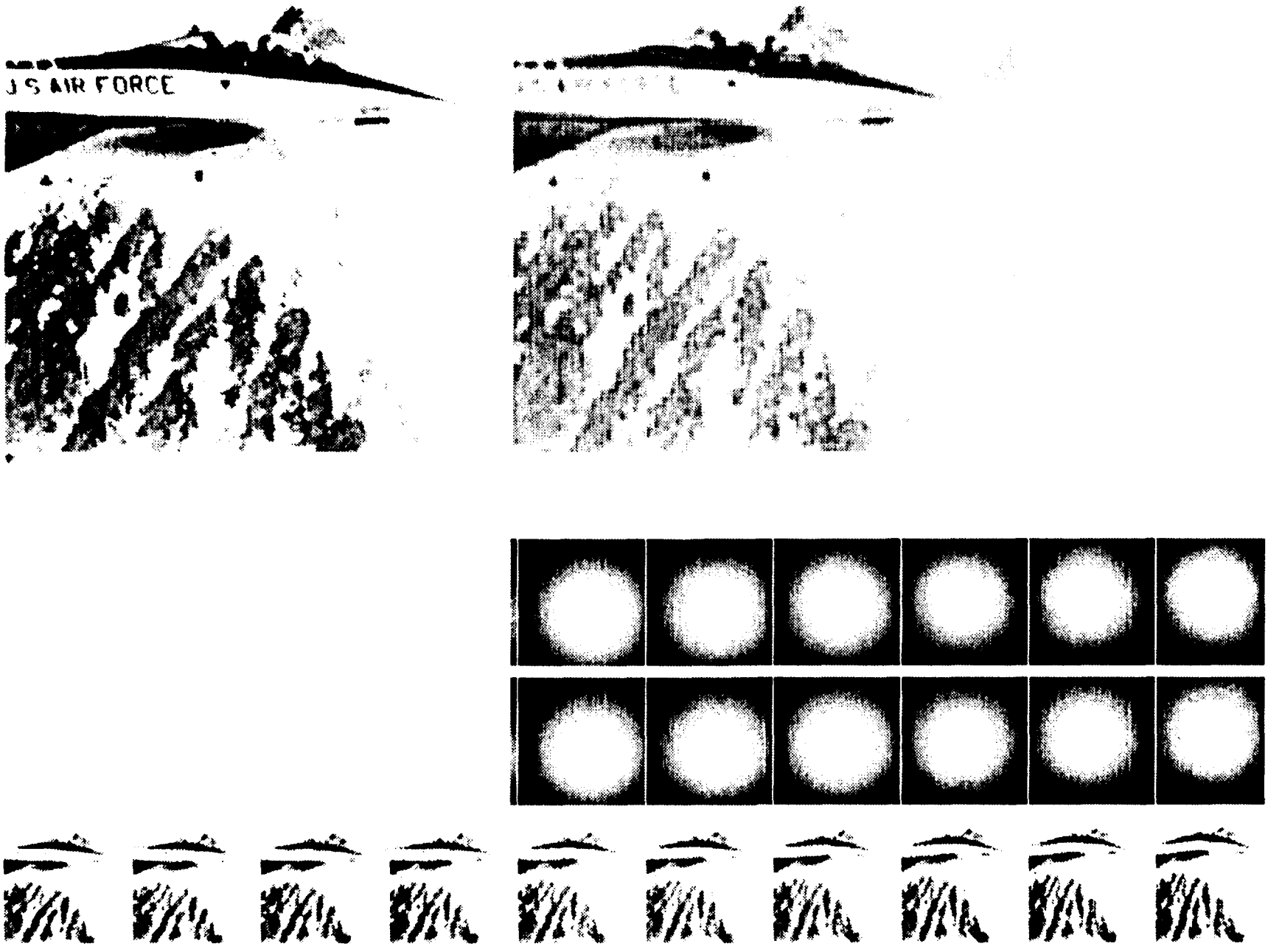

Figure 33

PICTURE – L.A. Times, 3/17/93

Video Leads to Plea of Guilty in Denny Case

■ **Courts:** Defendant Gary Williams, accused of rifling through trucker's pockets, opts against trial after he and lawyer view computer-enhanced tape.

ON THE RECORD

"They took a tape that was very blurred and made it very clear. It doesn't necessarily prove the case, but it certainly may have had an influence on the jury, and my client thought it in his best interest to accept the settlement."

—Defense attorney Arlene Binder on her client, Gary Williams, pleading guilty in the Reginald Denny beating case. B1

DENNY BEATING: The surprise introduction of a computer-enhanced video led one of the lesser defendants in the Reginald Denny beating case to plead guilty to all charges against him. B1

Figure 34